EXACT SOLUTIONS OF THE MHD THREE-DIMENSIONAL CASSON FLOW OF A TERNARY HYBRID NANOFLUID OVER A POROUS STRETCHING/SHRINKING SURFACE WITH MASS TRANSPIRATION

M. I. Kopp[1] (ID), U. S. Mahabaleshwar[2] (ID), L. M. Pérez[3] (ID)

[1]*Institute for Single Crystals, NAS Ukraine, 60, ave. Nauky, Kharkiv, UA–61072, Ukraine,*
[2]*Department of Studies in Mathematics, Shivagangotri,*
Davangere University, Davangere, 577007, India,
[3]*Departamento de Física, FACI, Universidad de Tarapacá, Casilla, 7D, Arica, Chile*

In this paper, the three-dimensional Casson flow of a ternary hybrid nanofluid over a porous linearly stretching/shrinking surface in the presence of an external magnetic field is considered. The surface deformation process is described by introducing two parameters of stretching/shrinking in the lateral directions. Using similarity transformations, the basic set of nonlinear partial differential equations is converted into ordinary differential equations. An exact analytical solution to this boundary value problem is obtained. The influence of the Casson parameter, magnetic field, porosity medium, and stretching/shrinking parameter, taking into account mass transpiration, on the velocity profiles and the skin friction coefficients is considered in detail. It has been established that the results obtained in some limited cases are in excellent agreement with the available data. Tables show the new results for the skin friction coefficients in the lateral directions (x and y) for different variants of surface deformation.

Key words: Casson flow, ternary hybrid nanofluid, mass transpiration, analytical solution.

I. INTRODUCTION

Recently, the problem of the boundary flow of non-Newtonian fluids has attracted more and more attention. Most industrial fluids, such as polymer solutions and melts, paints and varnishes, fuels and lubricants, drilling fluids, liquid petroleum products, and so on, are non-Newtonian. The Casson fluid, which he introduced in 1995 to describe the flow of viscoelastic fluids, is the most widely used model for non-Newtonian fluids. In the Casson viscous fluid flow model, the shear stresses are greater than the yield strength. If the shear stresses are less than the yield strength, then the Casson fluid behaves like a solid. Examples of Casson fluid in the food industry are jelly, tomato sauce, honey, concentrated fruit juices, and, in medicine, human blood. The flow of a viscous fluid over a stretching/shrinking surface plays an important role in processes such as the melting of high molecular weight polymers and the production of glass, fiber, plastic, and rubber materials.

Sakiadis [1] and Tsou *et al.* [2] pioneered studies of boundary layer flow on solid surfaces. Crane [3] found an analytical solution for a two-dimensional stationary flow in a boundary layer caused by an expanding surface whose velocity varies linearly with distance from a fixed point. Numerous researchers have been motivated by these papers [1–3] to investigate various aspects of this problem, whether by combining the problem with heat and mass transfer, MHD, chemical processes, suction/injection, mass transpiration, non-Newtonian fluids, or other different scenarios. Studies on two-dimensional boundary layer flows caused by stretching surfaces are extensively studied with various fluids under different conditions due to their numerous applications. There are a huge amount of articles published about this issue for a

long time. Therefore, in the review part of this study, the main focus is on the articles devoted to three-dimensional MHD flows of a non-Newtonian (Casson) fluid over a stretching/shrinking surface.

Wang [4] obtained an exact similarity solution of the Navier-Stokes equations for a three-dimensional flow of a boundary layer of a viscous fluid over a flat surface that is stretched with a linear velocity in two lateral directions. The concepts presented in this paper provided inspiration for the study of three-dimensional flows under more complex physical circumstances. The problem of steady laminar three-dimensional magnetohydrodynamic (MHD) boundary layer flow and heat transfer over a stretching surface in a viscoelastic fluid was investigated by Ahmad and Nazar [5]. They obtained coupled non-linear ordinary differential equations to describe the flow, which they solved numerically using the finite difference scheme known as the Kellerbox method. Ramzan *et al.* [6] investigated the three-dimensional flow of a viscoelastic fluid, taking into account the Soret and Dufour effects. In [6], solution expressions of velocity, temperature and nanoparticle concentration are computed via homotopy analysis method (HAM). Ashraf *et al.* [7] considered the heat and mass transfer effects in the three-dimensional flow of a Maxwell fluid over a stretching surface with convective boundary conditions. Nadeem *et al.* [8] investigated the Casson fluid flow on a permeable sheet caused by sheet stretching in the x and y directions in a transverse magnetic field. In a later study, Nadeem *et al.* [9] extended the study to a Casson nanofluid over a linearly stretching sheet, taking into account surface convective conditions. Mahanta and Shaw [10] investigated a three-dimensional Casson fluid flow past a porous linearly stretching sheet, introducing

a convective boundary condition at the surface where the fluid's thermal conductivity varies linearly concerning temperature. They used the Spectral Relaxation Method (SRM) to solve the governing equations, and computations were performed for the velocity and temperature fields for different parameters. Krishna Murthy [11] solved MHD Casson fluid flow past a porous, linearly stretching surface with wall mass transfer analytically. In [11] the fluid velocity and skin friction coefficient were calculated, and it was demonstrated that increasing the Casson and porosity parameters suppressed the velocity field.

With the development of nanotechnology, a new type of liquid has arisen, the so-called "nanofluids" [12]. A nanofluid is a colloidal suspension of a nanoscale particle in a base fluid. Metals, oxides, carbides, and carbon nanotubes are commonly used as nanoparticles, while water and ethylene glycol are used as the base fluid. Nanofluids have a greater thermal conductivity than regular fluids, which is needed for the efficient transfer of thermal energy. Nanofluids can take the place of current refrigerants in a number of sectors, including energy, electronics, transportation, and manufacturing. In this regard, researchers have been particularly interested in the applications of nanofluids since the discovery of this original concept. The suspension of many nanoparticles in the base fluid results in the creation of a novel type of nanofluid known as a hybrid nanofluid. A new class of nanofluids has emerged, consisting of three solid nanoparticles distributed in an ordinary liquid. The term "ternary hybrid nanofluid" is commonly used to describe these fluids [13]. Recent studies [14–16] by numerous researchers looked at the thermal properties of ternary fluid.

Madhusudan *et al.* [17] numerically studied the convective, three-dimensional, electrically conducting Casson nanofluid flow over an exponentially stretching sheet embedded in a saturated porous medium and subjected to thermal as well as solute slip in the presence of an externally applied transverse magnetic field. Ibrahim and Anbessa [18] investigated the three-dimensional MHD mixed convection flow of Casson nanofluid over an exponentially stretching sheet using the impacts of Hall and ion slip currents, taking into account thermal radiation and the heat source. Vishalakshi *et al.* [19] obtained exact analytical solutions for the three-dimensional flow of a non-Newtonian fluid due to a porous stretching/shrinking sheet. The importance of paper [19] is to examine the problem analytically and find the domain in terms of mass transpiration that is used in the heat transfer equation to analyze the heat equation. Mahabaleshwar *et al.* [20] conducted an investigation of the exact analytical solution for velocity and concentration field for 3D MHD flow viscoelastic HNF due to a porous sheet that stretched/shrunk along both x and y axes with linear velocity and Navier slip. Exact analytical solutions in exponential and hypergeometric form for velocity and concentration fields were obtained in [20]. The flow of Marangoni convection MHD Casson fluid with carbon nanotubes under the effects of transpiration and radi-

ation was analyzed by Vishalakshi *et al.* [21]. The ordinary differential equations (ODEs) obtained in [21] are solved analytically, first using the momentum equation to obtain the solution domain, and then using this domain, the energy equation is solved to obtain the temperature profile in terms of the Laguerre polynomial. Recently, Khan *et al.* [22] found an exact solution of a Casson fluid flow induced by dust particles with hybrid nanofluid over a stretching sheet under a Lorentz force. They obtained the analytical solutions of momentum equations for the fluid and dust phases velocities of the normal nanofluid (Fe_3O_4/H_2O) and hybrid nanofluid (Fe_3O_4-MWCNT/H_2O).

Most of the above investigations are based on numerical solutions. Therefore, inspired by the above-mentioned articles, the present work is devoted to an analytical study of the three-dimensional MHD Casson flow of a ternary hybrid nanofluid due to stretching/shrinking of a porous surface. In contrast to previous works [19–21], the novelty of this work is an analytical consideration of the problem that takes into account various options for the deformation caused by stretching/shrinking of a porous surface in the lateral directions x and y. Using various physical parameters, the problem is checked precisely, and velocity profiles and skin friction coefficients in directions x and y are examined. In this work, we will study in detail the effect of the volume concentration of nanoparticles of lower density on the flow of a ternary hybrid nanofluid over a stretching/shrinking sheet under conditions of mass transpiration. Unlike work [19], we will examine the area of exact solutions for velocity profiles depending on the mass transpiration parameter. Furthermore, in contrast to [19], we will compare the new findings for the skin friction coefficients in both lateral directions with those of other studies that are well-known in the literature. All newly discovered results will be displayed graphically and in tables.

II. PROBLEM STATEMENT

Let us consider a laminar flow of an incompressible three-dimensional (3D) flow of a ternary hybrid nanofluid (for example, TiO_2–SiO_2–Al_2O_3–H_2O [14]) flowing around a stretching/shrinking porous layer. It is assumed that the surface is stretched/shrunk along the x and y axes, and the fluid is sucked ($V_c < 0$) or injected ($V_c > 0$) along the z axis (mass transpiration). In the case where ($V_c = 0$), we have an impermeable surface. An external constant magnetic field B_0 is applied to the fluid flow, and the induced magnetic field is considered negligible. Fig. 1 illustrates the physical model's flow. It is assumed that the sheet has linear velocities along the xy plane: $u = d_1 a x$ and $v = d_2 b y$, respectively; (d_1, d_2) are constant stretch and shrink parameters, with (d_1, d_2) > 0 indicating a stretched sheet, (d_1, d_2) < 0 indicating a shrinking sheet, and (d_1, d_2) = 0 indicating a static sheet.
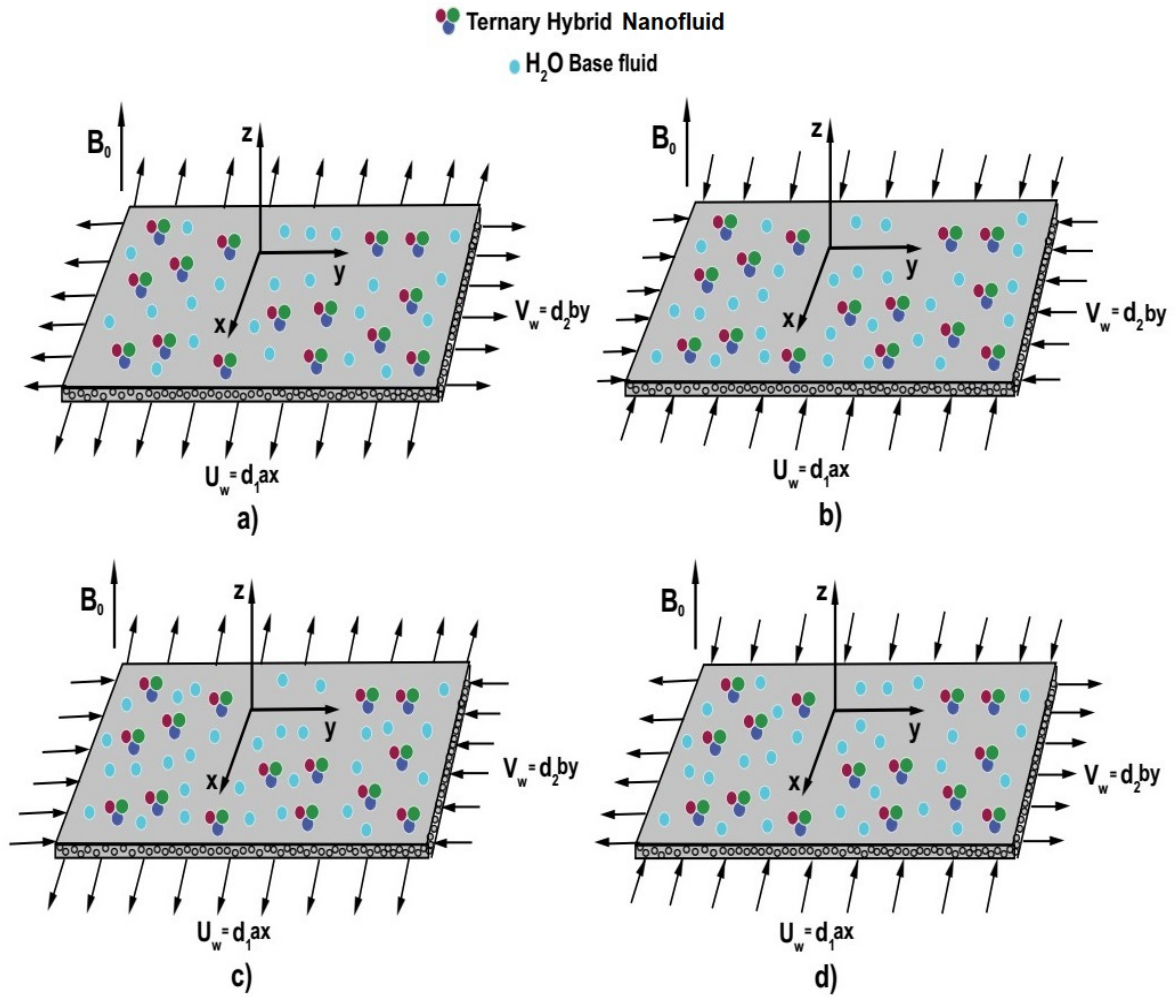
Fig. 1. The physical model for stretching/shrinking of a porous surface: a) stretching-stretching $(d_1 > 0, d_2 > 0)$; b) shrinking-shrinking $(d_1 < 0, d_2 < 0)$; c) stretching-shrinking $(d_1 > 0, d_2 < 0)$; d) shrinking-stretching $(d_1 < 0, d_2 > 0)$

Based on these assumptions, the three-dimensional incompressible Casson ternary hybrid nanofluid boundary layer equations are as follows:

$$\frac{\partial u}{\partial x} + \frac{\partial v}{\partial y} + \frac{\partial w}{\partial z} = 0, \qquad (1)$$

$$u\frac{\partial u}{\partial x} + v\frac{\partial u}{\partial y} + w\frac{\partial u}{\partial z} \qquad (2)$$

$$= \frac{\mu_{\text{thf}}}{\rho_{\text{thf}}}\left(1 + \frac{1}{\Lambda}\right)\frac{\partial^2 u}{\partial z^2} - \frac{\mu_{\text{thf}}}{K\rho_{\text{thf}}}u - \frac{\sigma_{\text{thf}}}{\rho_{\text{thf}}}B_0^2 u,$$

$$u\frac{\partial v}{\partial x} + v\frac{\partial v}{\partial y} + w\frac{\partial v}{\partial z} \qquad (3)$$

$$= \frac{\mu_{\text{thf}}}{\rho_{\text{thf}}}\left(1 + \frac{1}{\Lambda}\right)\frac{\partial^2 v}{\partial z^2} - \frac{\mu_{\text{thf}}}{K\rho_{\text{thf}}}v - \frac{\sigma_{\text{thf}}}{\rho_{\text{thf}}}B_0^2 v.$$

The following are the boundary conditions for the investigated model:

$$u = U_w(x) = d_1 ax, \ v = V_w(y) = d_2 by, \ w = w_0 \quad (4)$$
$$\text{at} \quad z = 0$$

$$u \to 0, \quad v \to 0 \quad \text{at} \quad z \to \infty \qquad (5)$$

Here μ_{thf} is the dynamic viscosity of the ternary hybrid nanofluids, ρ_{thf} is the density of the ternary hybrid nanofluids, σ_{thf} the electrical conductivity, Λ is the Casson (non-Newtonian) fluid parameter, K is the permeability of a porous medium, B_0 is the magnetic induction, a and b are stretching rates along x and y axes.

In equations (2)–(3), the subscript "thf" denotes the physical quantities for the ternary hybrid nanofluid, which are defined below as

1. Density

$$\rho_{\text{thf}} = (1 - \phi_3)\big\{(1 - \phi_2)[(1 - \phi_1)\rho_f + \phi_1\rho_{s1}] + \phi_2\rho_{s2}\big\}$$
$$+\phi_3\rho_{s3}. \qquad (6)$$

2. Dynamic viscosity

$$\frac{\mu_{\text{thf}}}{\mu_f} = \frac{1}{(1 - \phi_1)^{2.5}(1 - \phi_2)^{2.5}(1 - \phi_3)^{2.5}}. \qquad (7)$$

3. Electrical conductivity

$$\frac{\sigma_{\text{thf}}}{\sigma_{\text{hf}}} = \frac{(1+2\phi_3)\sigma_{s3} + (1-2\phi_3)\sigma_{\text{hnf}}}{(1-\phi_3)\sigma_{s3} + (1+\phi_3)\sigma_{\text{hnf}}}, \text{ where}$$

$$\frac{\sigma_{\text{hnf}}}{\sigma_{\text{nf}}} = \frac{(1+2\phi_2)\sigma_{s2} + (1-2\phi_2)\sigma_{\text{nf}}}{(1-\phi_2)\sigma_{s2} + (1+\phi_2)\sigma_{\text{nf}}},$$

$$\text{and} \quad \frac{\sigma_{\text{nf}}}{\sigma_{\text{f}}} = \frac{(1+2\phi_1)\sigma_{s1} + (1-2\phi_1)\sigma_{\text{f}}}{(1-\phi_1)\sigma_{s1} + (1+\phi_1)\sigma_{\text{f}}}. \tag{8}$$

Here ρ_{f} is the density of the base fluid, σ_{f} is the electrical conductivity of the base fluid. The subscripts $(1, s1), (2, s2),$ and $(3, s3)$ denote the characteristics of nanoparticles TiO_2, SiO_2, and Al_2O_3, respectively. Table 1 shows the physical constants for nanoparticles and base fluid.

The partial differential equations (1)–(3) are transformed into ordinary differential equations through similarity transformation (see, for example, [19]):

$$u = axf'(\eta), \quad v = ayg'(\eta),$$

$$w = -\sqrt{a\nu_{\text{f}}}(f(\eta) + g(\eta)), \quad \eta = z\sqrt{\frac{a}{\nu_{\text{f}}}}, \tag{9}$$

where f, g are the dimensionless functions, η is the similarity variable, ν_{f} is the kinematic viscosity of the base fluid. Primes denote differentiation with regard to η in this context. Using the similarity transformations (9), the system PDEs (1)–(3) will transform into

$$\left(1 + \frac{1}{\Lambda}\right)\frac{\epsilon_1}{\epsilon_2}f''' + (f+g)f'' \tag{10}$$

$$- f'^2 - \left(\frac{\epsilon_3}{\epsilon_2}M + \frac{\epsilon_1}{\epsilon_2}\widetilde{K}\right)f' = 0$$

$$\left(1 + \frac{1}{\Lambda}\right)\frac{\epsilon_1}{\epsilon_2}g''' + (f+g)g'' \tag{11}$$

$$- g'^2 - \left(\frac{\epsilon_3}{\epsilon_2}M + \frac{\epsilon_1}{\epsilon_2}\widetilde{K}\right)g' = 0$$

and the related boundary conditions (4)–(5) are transformed as follows:

$$f'(0) = d_1, \quad f(0) = V_c = -\frac{w_0}{\sqrt{a\nu_{\text{f}}}}, \quad g(0) = 0, \tag{12}$$

$$g'(0) = \frac{d_2b}{a} \quad \text{at} \quad \eta = 0$$

$$f'(\eta) \to 0, \quad g'(\eta) \to 0 \quad \text{at} \quad \eta \to \infty \tag{13}$$

In equations (10)–(11), the quantities $\epsilon_1, \epsilon_2, \epsilon_3$ are defined as

$$\epsilon_1 = \frac{\mu_{\text{thf}}}{\mu_{\text{f}}}, \quad \epsilon_2 = \frac{\rho_{\text{thf}}}{\rho_{\text{f}}}, \quad \epsilon_3 = \frac{\sigma_{\text{thf}}}{\sigma_{\text{f}}}, \tag{14}$$

Property	H_2O	TiO_2	SiO_2	Al_2O_3
$\rho \ [\text{kg} \cdot \text{m}^{-3}]$	997.1	4250	2270	6310
$\sigma \ [\text{S} \cdot \text{m}^{-1}]$	$5.5 \cdot 10^{-6}$	$2.4 \cdot 10^6$	$3.5 \cdot 10^6$	$5.96 \cdot 10^7$
$\phi \ [\%]$	No	$\phi_1 = 1\%$	$\phi_2 = 1\%$	$\phi_3 = 1\%$

Table 1. Physical properties of the nanoparticles and the base fluid [14]

and $M = \frac{B_0^2 \sigma_{\text{f}}}{a\rho_{\text{f}}}$ is the magnetic parameter, $\widetilde{K} = \frac{\nu_{\text{f}}}{aK}$ is the porosity parameter, V_c is the transpiration mass parameter.

III. ANALYTICAL SOLUTION

In this section, we will obtain the exact analytical solutions of equations (10)–(11) taking into account the boundary conditions (12)–(13). Based on Crane's [3] solution, we suggest that the general solution of equations (10)–(11) can be found in the exponential form:

$$f(\eta) = A_1 + A_2 e^{-\beta\eta},$$

$$g(\eta) = A_3 + A_4 e^{-\beta\eta}, \tag{15}$$

where A_1, A_2, A_3, A_4 are the arbitrary constants. Applying boundary conditions (12)–(13) to solutions (15), we obtain expressions for the coefficients:

$$A_1 = V_c + \frac{d_1}{\beta}, \ A_2 = -\frac{d_1}{\beta},$$

$$A_3 = \frac{d_2 b}{a}, \ A_4 = -\frac{d_2 b}{a}. \tag{16}$$

Substituting the values of the coefficients (16) into (15), we get the final form of the exact solution of equations (10)–(11):

$$f(\eta) = V_c + \frac{d_1}{\beta}\left(1 - e^{-\beta\eta}\right),$$

$$g(\eta) = \frac{d_2 b}{a\beta}\left(1 - e^{-\beta\eta}\right). \tag{17}$$

The value of the coefficient β can be easily determined using solutions (17). In order to do this, we substitute (17) into equations (10)–(11), as a result, we obtain, respectively, two equations of the following form:

$$q\frac{\epsilon_1}{\epsilon_2}\beta^2 - \beta V_c - d_1 - \frac{d_2 b}{a} \tag{18}$$

$$- \left(\frac{\epsilon_3}{\epsilon_1}M + \frac{\epsilon_1}{\epsilon_2}\widetilde{K}\right) + \frac{d_2 b}{a}e^{-\beta\eta} = 0,$$

$$q\frac{\epsilon_1}{\epsilon_2}\beta^2 - \beta V_c - d_1 - \frac{d_2 b}{a} \tag{19}$$

$$-\left(\frac{\epsilon_3}{\epsilon_1}M + \frac{\epsilon_1}{\epsilon_2}\widetilde{K}\right) + d_1 e^{-\beta\eta} = 0.$$

Then we multiply equation (18) by d_1, and equation (19) by $d_2 b/a$, and subtracting these equations from each other we get

$$\left(q\frac{\epsilon_1}{\epsilon_2}\beta^2 - \beta V_c - d_1 - \frac{d_2 b}{a} - \left(\frac{\epsilon_3}{\epsilon_1}M + \frac{\epsilon_1}{\epsilon_2}\widetilde{K}\right)\right)$$

$$\times \left(d_1 - \frac{d_2 b}{a}\right) = 0. \tag{20}$$

From (20), we find the quadratic equation for β:

$$\beta^2 - \frac{\epsilon_2}{q\epsilon_1}V_c\beta - \left(d_1 + \frac{d_2 b}{a} + \frac{\epsilon_3}{\epsilon_1}M + \frac{\epsilon_1}{\epsilon_2}\widetilde{K}\right)\frac{\epsilon_2}{q\epsilon_1} = 0, \tag{21}$$

where β is determined by solving the quadratic equation (21) and given in the form

$$\beta = \frac{V_c\epsilon_2}{2q\epsilon_1} \pm \sqrt{\frac{V_c^2\epsilon_2^2}{4q^2\epsilon_1^2} + \frac{\epsilon_2}{q\epsilon_1}(d_1 + d_2 c) + \frac{\epsilon_3}{q\epsilon_1}M + \frac{\widetilde{K}}{q}},$$

$$c = \frac{b}{a}, \quad q = 1 + \frac{1}{\Lambda}. \tag{22}$$

Obviously, we need only positive values of $\beta > 0$.

By differentiating expression (17) with respect to η, we can determine the velocity profiles in the x and y directions:

$$f'(\eta) = d_1 e^{-\beta\eta}, \quad g'(\eta) = \frac{d_2 b}{a}e^{-\beta\eta} \tag{23}$$

The skin friction coefficient $C_{\rm f}$ on the surface along the x and y axes is expressed as follows (see, for example, [8]):

$$C_{fx}\sqrt{Re_x} = \frac{\mu_{\rm thf}}{\mu_{\rm f}}\left(1 + \frac{1}{\Lambda}\right)f''(0),$$

$$\tag{24}$$

$$C_{fy}\sqrt{Re_x} = \frac{\mu_{\rm thf}}{\mu_{\rm f}}\left(1 + \frac{1}{\Lambda}\right)\left(\frac{y}{x}\right)g''(0),$$

where $Re_x = U_w x/\nu_{\rm f}$ is the local Reynolds number, $f''(0) = -d_1\beta$, $g''(0) = -d_2 c\beta$.

IV. RESULTS AND DISCUSSION

In this section, analytical solutions for velocity profiles $f'(\eta)$, $g'(\eta)$ and solution domain of β are discussed as a function of changes in various physical parameters $\Lambda, M, \widetilde{K}$. The results obtained are presented graphically as shown in Figs. 2-5 for four variants of surface

deformation (see Fig. 1). The range of the following parameters is taken into account for the calculations:

$$\Lambda = (1, 3, \infty), \ M = (0.5, 1, 1.5),$$

$$\widetilde{K} = (0.5, 1, 1.5, 2, 2.5),$$

$$V_c = [-10\ldots 10], \quad \phi_1 = \phi_3 = 0.01, \quad \phi_2 = (0.01, 0.5).$$

Figure 2 shows dependences of the solution domain of β on mass transpiration (suction/injection) V_c for four variants of surface deformation (see Fig. 1) at $\phi_1 = \phi_2 = \phi_3 = 0.01$, $c = 0.5$ and different values of $\Lambda, M, \widetilde{K}$. We notice that for $c = 0$, we get the case of a one-dimensional linear stretching/shrinking sheet. If $c = 1$, the sheet will stretch/shrink with the same ratio in both directions. We take the ratio parameter c other than 0 or 1, i.e. $c = 0.5$, then the flow behavior along both directions will be different.

As can be seen from Fig. 2,a–b, an increase in the Casson parameter Λ leads to an increase in β. The case $\Lambda = \infty$ corresponds to a Newtonian fluid. For the mass suction parameter ($V_c < 0$), the values β are low and are in the range about $(0.1\ldots 1.2)$, and for a case of the mass injection parameter ($V_c > 0$), a growth of Λ leads to β reaching higher positive values. Furthermore, we can see from Fig. 2,a–b that different variants of surface deformation have a different effect on the solution domain of β. The value of the parameter β is greater for a stretching/stretching surface than for other variants of surface deformation. Figs. 2,c–d and 2,e–f show that with the growth of the parameters M and $\widetilde{K}$, the value of β increases significantly in the case of mass injection ($V_c > 0$). In this case, the value of the β parameter for the stretching/stretching surface is also greater than that for other variants of surface deformation.

The effects of the non-Newtonian parameter Λ on the velocity profiles $f'(\eta)$, $g'(\eta)$ for various variants of surface deformation are shown in Fig. 3. Fig. 3,a, it can be seen that with an increase in the parameter Λ, the resistance to the fluid flow on the stretching/stretching surface increases. This leads to a decrease in the thickness of the boundary layer. Furthermore, Fig. 3,a depicts the effect of increasing the fluid flow velocity with an increase in the volume fraction of less dense nanoparticles ($\phi_{\rm SiO_2} = 0.01 \to \phi_{\rm SiO_2} = 0.5$). Because the less dense nanoparticles pull the fluid along with them in their direction of motion, the velocity of the fluid flow increases. An increase in the parameter Λ in the case of a shrinking/shrinking surface leads to a decrease in the absolute values of $f'(\eta)$ and $g'(\eta)$, as shown in Fig. 3,b. However, while a surface is shrinking in two lateral directions, the increase in the volume fraction of less dense nanoparticles ($\phi_{\rm SiO_2} = 0.01 \to \phi_{\rm SiO_2} = 0.5$) resists the fluid's flow, which causes the absolute values of $f'(\eta)$ and $g'(\eta)$ to decrease. Figs. 3,c and 3,e show the effect of the Casson parameter Λ on velocity profiles $f'(\eta)$ and $g'(\eta)$ for the cases of stretching/shrinking and shrinking/stretching surfaces, respectively. In these figures, we

also observe a decrease in the absolute values of $f'(\eta)$ and $g'(\eta)$ with an increase in parameter Λ.

A similar behavior of velocity profiles $f'(\eta)$ and $g'(\eta)$ can be seen in Fig. 4, which shows that the Lorentz force increases in accordance with the increase in the values of the magnetic parameter M. As a result, there is some resistance to the fluid flow, which leads to a decrease in the flow velocity profiles. On the stretching/stretching surface, we also see the effect of increasing the fluid flow velocity (see Fig. 4,a) with an increase in

the volume fraction of less dense nanoparticles ($\phi_{\mathrm{SiO_2}} = 0.01 \rightarrow \phi_{\mathrm{SiO_2}} = 0.5$). On the other hand, on the shrinking/shrinking surface, we also see the effect of a decrease in the absolute value of the fluid flow velocity (see Fig. 4,b) with an increase in the volume fraction of less dense nanoparticles ($\phi_{\mathrm{SiO_2}} = 0.01 \rightarrow \phi_{\mathrm{SiO_2}} = 0.5$). In the cases of stretching-shrinking and shrinking-stretching surfaces, Figs. 4,c and 4,d show a decrease in the absolute values of $f'(\eta)$ and $g'(\eta)$ with increasing magnetic parameter M.
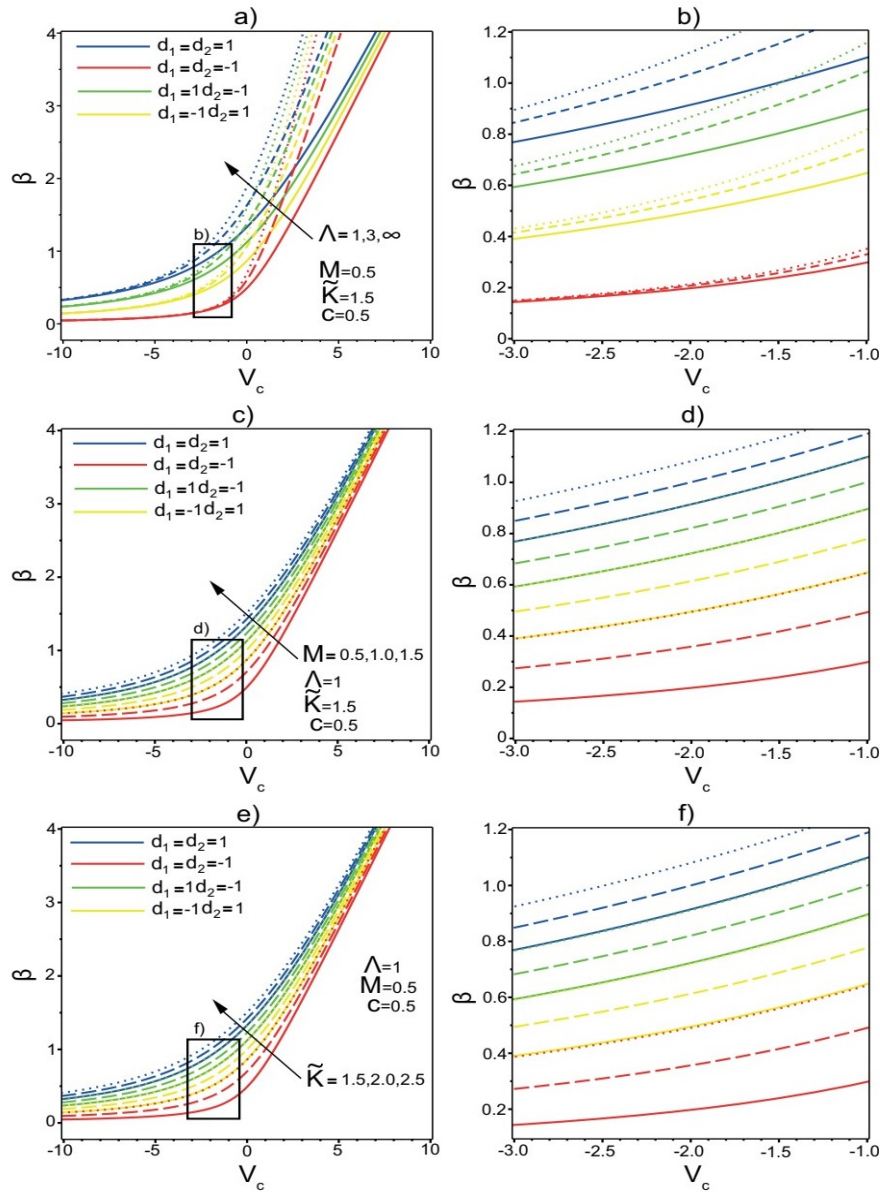

Fig. 2. The solution domain for β at various values of Casson parameter Λ (a-b), magnetic parameter M (c-d) and porosity parameter $\widetilde{K}$ (e-f) as a function of the mass transpiration V_c for a stretching/stretching ($d_1 = 1, d_2 = 1$) surface, shrinking-shrinking ($d_1 = -1, d_2 = -1$) surface, stretching-shrinking ($d_1 = 1, d_2 = -1$) surface, shrinking-stretching ($d_1 = -1, d_2 = 1$) surface
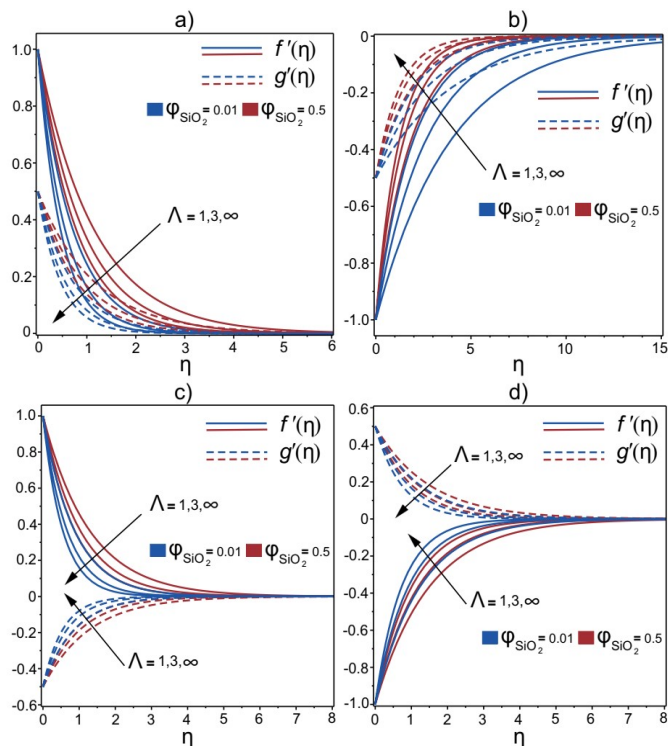
Fig. 3. Influence of Λ on velocity profiles $f'(\eta)$ and $g'(\eta)$ at fixed parameters $M = \widetilde{K} = c = 0.5$ and $V_c = 1$ for a) stretching/stretching ($d_1 = 1, d_2 = 1$) surface; b) shrinking-shrinking ($d_1 = -1, d_2 = -1$) surface; c) stretching-shrinking ($d_1 = 1, d_2 = -1$) surface; d) shrinking-stretching ($d_1 = -1, d_2 = 1$) surface
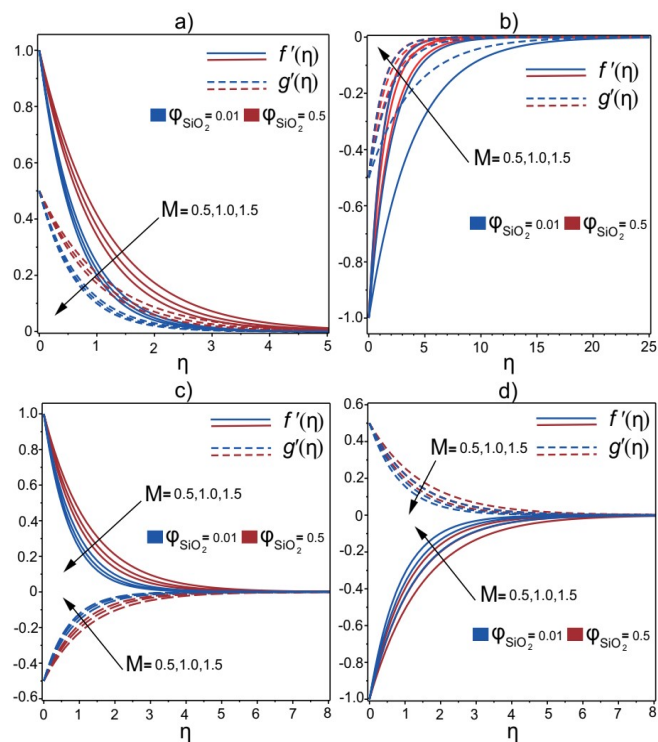
Fig. 4. Effect of M on velocity profiles $f'(\eta)$ and $g'(\eta)$ at fixed parameters $\Lambda = 1, \widetilde{K} = c = 0.5$ and $V_c = 1$ for a) stretching/stretching ($d_1 = 1, d_2 = 1$) surface; b) shrinking-shrinking ($d_1 = -1, d_2 = -1$) surface; c) stretching-shrinking ($d_1 = 1, d_2 = -1$) surface; d) shrinking-stretching ($d_1 = -1, d_2 = 1$) surface

Fig. 5. Effect of $\widetilde{K}$ on velocity profiles $f'(\eta)$ and $g'(\eta)$ at fixed parameters $\Lambda = 1, M = c = 0.5$ and $V_c = 1$ for a) stretching/stretching ($d_1 = 1, d_2 = 1$) surface; b) shrinking-shrinking ($d_1 = -1, d_2 = -1$) surface; c) stretching-shrinking ($d_1 = 1, d_2 = -1$) surface; d) shrinking-stretching ($d_1 = -1, d_2 = 1$) surface
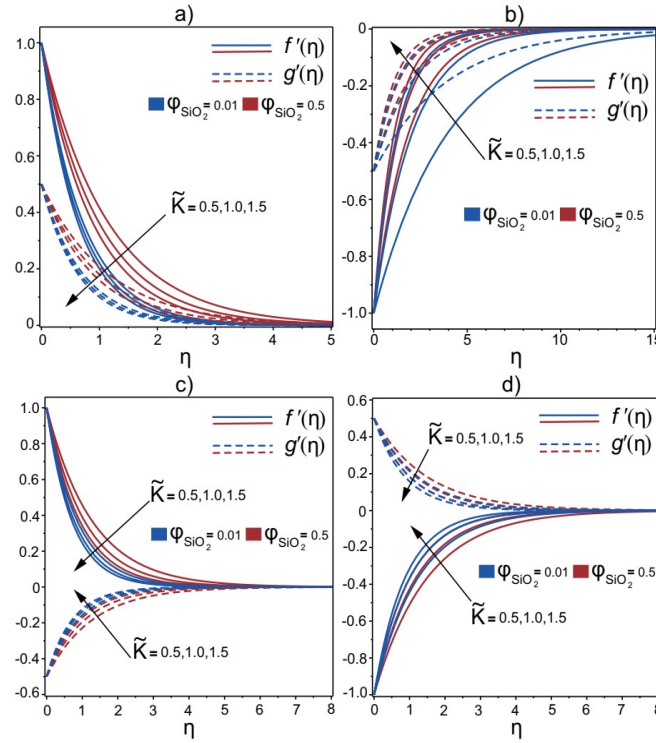
The conclusions made above when analyzing the influence of the Casson parameters Λ and the magnetic field M on the velocity profiles in the lateral directions of the surface remain valid for the porosity parameter as well. From Fig. 5, it can be seen that with an increase in the values of the porosity parameter $\widetilde{K}$ in the boundary layer, the velocities decrease in both directions. Therefore, the thickness of the boundary layer also decreases at higher values of $\widetilde{K}$.

Table 2 compares the analytical results obtained from expressions (24) for local skin friction coefficients $-f''(0), -g''(0)$ under the following conditions

$$V_c = 0, \quad \widetilde{K} = 0, \quad \phi_1 = \phi_2 = \phi_3 = 0, \quad d_1 = d_2 = 1$$

to the known numerical results of Ahmad and Nazar [5], Nadeem *et al.* [8], and Vajravelu *et al.* [23]. Table 2 shows that a good agreement is established between the exact solution (24) and the available numerical results [5, 8, 23].

Λ	M	c	$-f''(0)$ numerical results	$-g''(0)$ numerical results	$-f''(0)$ exact solutions	$-g''(0)$ exact solutions
∞	0	0	1.0000 [23] 1.0042 [5],[8]	0	1.0000	0
1	0	0	0.7071 [23]	0	0.7071	0
2	0	0	0.8164 [23]	0	0.8164	0
3	0	0	0.8660 [23]	0	0.8660	0
4	0	0	0.8944 [23]	0	0.8944	0
∞	0	0.5	1.0932 [5],[8]	0.4653 [5],[8]	1.2247	0.6123
∞	10	0.5	3.3420 [5],[8]	1.6459 [5],[8]	3.3911	1.6955
∞	100	0.5	10.058 [5],[8]	5.0208 [5],[8]	10.074	5.0373

Table 2. A comparison of exact solutions for skin friction coefficients $-f''(0)$ and $-g''(0)$ with numerical results [5, 8, 23]

Λ	M	$\widetilde{K}$	$-f''(0)$ $\phi_{\mathrm{SiO_2}} = 0.01$	$-g''(0)$ $\phi_{\mathrm{SiO_2}} = 0.01$	$-f''(0)$ $\phi_{\mathrm{SiO_2}} = 0.5$	$-g''(0)$ $\phi_{\mathrm{SiO_2}} = 0.5$
1	0.5	0.5	1.4086	0.7043	0.8765	0.4382
3	0.5	0.5	1.8124	0.9062	1.0951	0.5475
∞	0.5	0.5	2.1804	1.0902	1.2859	0.6429
1	1.0	0.5	1.5137	0.7568	0.9806	0.4903
1	1.5	0.5	1.6106	0.8053	1.0739	0.5369
1	0.5	1.0	1.5123	0.7561	1.0191	0.5095
1	0.5	1.5	1.6080	0.8040	1.1429	0.5714

Table 3. $-f''(0)$ and $-g''(0)$ values for a stretching-stretching surface ($d_1 = d_2 = 1$)

Λ	M	$\widetilde{K}$	$-f''(0)$ $\phi_{\mathrm{SiO_2}} = 0.01$	$-g''(0)$ $\phi_{\mathrm{SiO_2}} = 0.01$	$-f''(0)$ $\phi_{\mathrm{SiO_2}} = 0.5$	$-g''(0)$ $\phi_{\mathrm{SiO_2}} = 0.5$
1	0.5	0.5	-0.2545	-0.1272	-0.5395	-0.2697
3	0.5	0.5	-0.3818	-0.1909	-0.6838	-0.3419
∞	0.5	0.5	-0.5090	-0.2545	-0.8125	-0.4062
1	1.0	0.5	-0.4959	-0.2479	-0.7019	-0.3509
1	1.5	0.5	-0.8129	-0.4064	-0.8304	-0.4152
1	0.5	1.0	-0.4884	-0.2442	-0.7563	-0.3781
1	0.5	1.5	-0.8065	-0.4032	-0.9194	-0.4597

Table 4. $-f''(0)$ and $-g''(0)$ values for a shrinking-shrinking surface ($d_1 = d_2 = -1$)

Λ	M	$\widetilde{K}$	$-f''(0)$ $\phi_{\mathrm{SiO_2}} = 0.01$	$-g''(0)$ $\phi_{\mathrm{SiO_2}} = 0.01$	$-f''(0)$ $\phi_{\mathrm{SiO_2}} = 0.5$	$-g''(0)$ $\phi_{\mathrm{SiO_2}} = 0.5$
1	0.5	0.5	1.1616	-0.5808	0.7821	-0.3910
3	0.5	0.5	1.5144	-0.7572	0.9798	-0.4899
∞	0.5	0.5	1.8415	-0.9207	1.1531	-0.5765
1	1.0	0.5	1.2920	-0.6460	0.8982	-0.4491
1	1.5	0.5	1.4078	-0.7039	0.9999	-0.4999
1	0.5	1.0	1.2903	-0.6451	0.9404	-0.4702
1	0.5	1.5	1.4047	-0.7023	1.0740	-0.5370

Table 5. $-f''(0)$ and $-g''(0)$ values for a stretching-shrinking surface ($d_1 = 1, d_2 = -1$)

Λ	M	$\widetilde{K}$	$-f''(0)$ $\phi_{\mathrm{SiO_2}} = 0.01$	$-g''(0)$ $\phi_{\mathrm{SiO_2}} = 0.01$	$-f''(0)$ $\phi_{\mathrm{SiO_2}} = 0.5$	$-g''(0)$ $\phi_{\mathrm{SiO_2}} = 0.5$
1	0.5	0.5	-0.8147	0.4073	-0.6732	0.3366
3	0.5	0.5	-1.1024	0.5512	-0.8468	0.4234
∞	0.5	0.5	-1.3792	0.6896	-0.9999	0.4949
1	1.0	0.5	-1.0077	0.5038	-0.8067	0.4033
1	1.5	0.5	-1.1606	0.5803	-0.9194	0.4597
1	0.5	1.0	-1.0054	0.5027	-0.8538	0.4269
1	0.5	1.5	-1.1566	0.5783	-0.9999	0.4999

Table 6. $-f''(0)$ and $-g''(0)$ values for a shrinking-stretching surface ($d_1 = -1, d_2 = 1$)

Next, we study the influence of the non-Newtonian (Casson) parameter Λ, the magnetic field M, the porosity $\widetilde{K}$, and the expansion-shrinkage coefficients (d_1, d_2) on the local skin friction coefficients $-f''(0), -g''(0)$ for a ternary hybrid nanofluid TiO_2-SiO_2-Al_2O_3-H_2O. Numerical values of F and H for different values of $\Lambda, M, \widetilde{K}, \phi_2, d_1$, and d_2 at $c = 0.5, V_c = 1$ were obtained from exact solutions (17) and presented in Tabs. 3-6. From the results of Tables 3-6, it can be seen that at the limit of the Newtonian fluid ($\Lambda = \infty$), the skin friction coefficients of the hybrid nanofluid in the x and y directions are higher compared to the non-Newtonian fluid for various types of surface deformation and in the case of an increased volume fraction of less dense nanoparticles $\phi_{SiO_2} = 0.5$. Furthermore, increasing the magnetic parameter M and the porosity parameter $\widetilde{K}$ reduces the fluid flow rate, causing the absolute values of the skin friction coefficients in the x and y directions to increase.

V. CONCLUSIONS

This study has investigated for the first time the analytical solution of the three-dimensional MHD flow of the Casson ternary hybrid nanofluid over a linearly deformable surface with the effect of mass transpiration. Several linear stretching/shrinking sheet variants (see Fig. 1) in the lateral directions x and y are considered. Analytical expressions for the velocity and skin friction coefficients in the lateral directions are obtained using the flow arrangement of a ternary hybrid nanofluid considered. Under the condition of injection mass transpiration ($V_c = 1$), we investigated the impact of the Casson parameter Λ, magnetic field M, and medium porosity $\widetilde{K}$ on velocity profiles $f'(\eta)$ and $g'(\eta)$. The main results of this study are as follows:

1. The absolute values of skin friction coefficients in the lateral directions x and y increase in accordance with the growth of the parameters Λ, M, and $\widetilde{K}$ for various variants of the stretching/shrinking sheet.

2. For the cases of a stretching/stretching, stretching/shrinking, and shrinking/stretching sheet, the absolute values of the skin friction coefficients $-f''(0)$ and $-g''(0)$ decrease with an increase in the volume fraction of less dense nanoparticles.

3. In the case of a shrinking/shrinking sheet, the absolute values of skin friction coefficients $-f''(0)$ and $-g''(0)$ increase with an increase in the volume fraction of less dense nanoparticles.

The results of this work can be applied to numerous technological processes.

[1] B. C. Sakiadis, AIChE J. **7**, 221 (1961); https://doi.org/10.1002/aic.690070211.

[2] F. K. Tsou, E. M. Sparrow, R. J. Goldstein, Int. J. Heat Mass Transf. **10**, 219 (1967); https://doi.org/10.1016/0017-9310(67)90100-7.

[3] L. Crane, Z. Angew. Math. Phys. **21**, 645 (1970); https://doi.org/10.1007/BF01587695.

[4] C. Y. Wang, Phys. Fluids **27**, 1915 (1984); https://doi.org/10.1063/1.864868.

[5] K. Ahmad, R. Nazar, J. Sci. Technol. **3**, 33 (2011).

[6] M. Ramzan, S. Inam, S. A. Shehzad, Alex. Eng. J. **55**, 311 (2015); https://doi.org/10.1016/j.aej.2015.09.012.

[7] M. B. Ashraf, T. Hayat, M. S. Alhuthali, J. Aerosp. Eng. **29**, 04015065-1-8 (2016); https://doi.org/10.1061/(ASCE)AS.1943-5525.0000551.

[8] S. Nadeem, R. U. Haq, N. S. Akbar, Z. H. Khan, Alex. Eng. J. **52**, 577 (2013); https://doi.org/10.1016/j.aej.2013.08.005.

[9] S. Nadeem, R. U. Haq, N. S. Akbar, IEEE Trans. Nanotechnol. **13**, 108 (2014); https://doi.org/10.1109/TNANO.2013.2293735.

[10] G. Mahanta, S. Shaw, Alex. Eng. J. **54**, 653 (2015); https://doi.org/10.1016/j.aej.2015.04.014.

[11] M. Krishna Murthy, Int. J. Chem. Eng. Res. **41**, 29 (2016).

[12] S. U. S. Choi, in *Development and Applications of Non-Newtonian Flows*, Vol. 66, edited by D. A. Signier, H. P. Wang (ASME, New York, 1995), p. 99.

[13] T. Anusha, U. S. Mahabaleshwar, Y. Sheikhnejad, Transp. Porous Med. **142**, 333 (2021); https://doi.org/10.1007/s11242-021-01695-y.

[14] S. Manjunatha, V. Puneeth, B. J. Gireesha, A. J. Chamkha, J. Appl. Comput. Mech. **8**, 1279 (2022); https://doi.org/10.22055/JACM.2021.37698.3067.

[15] I. L. Animasaun, S. J. Yook, T. Muhammad, A. Mathew, Surf. Interfaces **28**, 101654 (2022); https://doi.org/10.1016/j.surfin.2021.101654.

[16] T. Maranna, U. S. Mahabaleshwar, M. I. Kopp, J. App. Comput. Mech. **9**(2), 487 (2023); https://doi.org/10.22055/jacm.2022.41405.3748.

[17] S. Madhusudan, S. Kharabela, P. S. Kumar, Karbala Int. J. Mod. Sci. **6**, 93 (2020); https://doi.org/10.33640/2405-609X.1462.

[18] W. Ibrahim, T. Anbessa, Hindawi Math. Probl. Eng. **2020**, Article ID 8656147 (2020); https://doi.org/10.1155/2020/8656147.

[19] A. B. Vishalakshi, U. S. Mahabaleshwar, I. E. Sarris, Micromachines **13**, 116 (2022); https://doi.org/10.3390/mi13010116.

[20] U. S. Mahabaleshwar *et al.*, Sustainability **14**, 7020 (2022); https://doi.org/10.3390/su14127020.

[21] A. B. Vishalakshi, U. S. Mahabaleshwar, M. Hatami, Sci. Rep. **12**, 16071 (2022); https://doi.org/10.1038/s41598-022-20532-w.

[22] U. Khan *et al.*, Waves Random Complex Media, published online: 25 July 2022; https://doi.org/10.1080/17455030.2022.2102689.

[23] K. Vajravelu *et al.*, Int. J. Appl. Comput. Math. **3**, 1619 (2017); https://doi.org/10.1007/s40819-016-0203-6.

ТОЧНІ РОЗВ'ЯЗКИ МГД ТРИВИМІРНОЇ ТЕЧІЇ КЕССОНА ПОТРІЙНОЇ ГІБРИДНОЇ НАНОРІДИНИ ПО ПОРИСТІЙ ПОВЕРХНІ РОЗТЯГУВАННЯ/СТИСНЕННЯ З МАСОВОЮ ТРАНСПІРАЦІЄЮ

М. Й. Копп[1], У. Ш. Магабалешвар[2], Л. М. Перес[3]

[1]*Інститут монокристалів, Національна академія наук України, просп. Науки, 60, Харків, 61001, Україна*

[2]*Факультет математики, Шівал'анл'отрі, Університет Даванл'ере, Індія, 577 007*

[3]*Факультет фізики, Університет Тарапака, бокс 7D, Аріка, Чилі*

У цій роботі розглянуто тривимірну кессонівську течію потрійної гібридної нанорідини по пористій поверхні, що лінійно розтягується/стискається за наявності зовнішнього магнітного поля. Деформацію поверхні описано введенням двох параметрів розтягування/стиснення в латеральних напрямках. За допомогою перетворень подібності базова система нелінійних диференційних рівнянь у часткових похідних перетворюється на прості диференційні рівняння. Отримано точний аналітичний розв'язок цієї крайової задачі. Докладно розглянуто вплив параметра Кессона, магнітного поля, пористості середовища та параметра розтягування/стиснення з урахуванням транспірації маси на профілі швидкості та коефіцієнти поверхневого тертя. Установлено, що результати, отримані в деяких обмежених випадках, чудово узгоджуються з наявними даними. У таблицях подано нові результати для коефіцієнтів поверхневого тертя в латеральних напрямках (x і y) для різних варіантів деформації поверхні.

Ключові слова: потік Кессона, потрійний гібридний нанофлюїд, масова транспірація, аналітичне рішення.